STRONG MOTION SIMULATION IN DOWNTOWN MASHIKI DURING 2016 KUMAMOTO EARTHQUAKE TO REPRODUCE THE DAMAGE BELT

J. Sun(1), H. Kawase(2), F. Nagashima(3), and S. Matsushima(4)

(1) *Ph.D. Candidate, Grad. School of Eng., Kyoto University, jikai.sun@sds.dpri.kyoto-u.ac.jp*
(2) *Program-Specific Professor, DPRI, Kyoto University, kawase@sere.dpri.kyoto-u.ac.jp*
(3) *Program-Specific Assistant Professor, DPRI, Kyoto University, nagashima@sere.dpri.kyoto-u.ac.jp*
(4) *Professor, DPRI, Kyoto University, matsushima@sds.dpri.kyoto-u.ac.jp*

Abstract

After the mainshock of the 2016 Kumamoto Earthquake, we conducted microtremor surveys twice in downtown Mashiki, Kumamoto Prefecture, Japan, where extremely heavy damage had occurred [1]. In the first observation which was conducted two weeks after the mainshock, we observed microtremors at 62 sites. We measured microtremors again at 35 sites in 2018 to get better quality microtremors and to fill the spatial gap of observation sites in the first survey. We used 15 to 20 minutes of these observed microtremors to obtain Microtremor Horizontal-to-Vertical Spectral Ratio (MHVR) by the Fast Fourier Transform (FFT).

We made a fundamental frequency map of MHVRs, and found that the northeastern side of the downtown area tends to have a higher frequency at around 4 Hz, while the southwestern side tends to have a frequency lower than 1 Hz. Next, we obtained pseudo Earthquake Horizontal-to-Vertical Spectral Ratio (pEHVR) converted from MHVR by using the EMR method [2], and we identified velocity structures to reproduce pEHVR by using Hybrid Heuristic Search method [3] at selected sites, where the quality of the observed microtremors was good. Finally, we got the velocity structures of Mashiki.

We simulated surface ground motions using the identified structures and the estimated seismic bedrock motions by the linear analysis (LA) and equivalent linear analysis (ELA) to see the effects of soil nonlinearity. Seismic bedrock motions were estimated by Nagashima and Kawase (2018) based on diffuse field concept. We made the estimated PGA and PGV distribution maps for both LA and ELA. We found the PGV distribution had close correlations with the observed damage belt of wooden houses in downtown Mashiki for the ELA case, while PGA and PGV showed too large values for the LA case.

Keywords: Damage Belt; Microtremor; Horizontal-to-Vertical Spectral Ratios; Site Amplification; Soil Nonlinearity

1. Introduction

On April 16, 2016, there occurred the mainshock of the 2016 Kumamoto Earthquake on the Kyushu island, Japan, the magnitude reported by the Japan Meteorological Agency (JMA) was M_{JMA} 7.3 [4]. This event caused severe damage of wooden buildings at the Downtown Mashiki, which is a small town located in the east of Kumamoto city and near the intersection of the Futagawa and Hinagu fault zones. JMA seismic intensity was 7 at Mashiki during the mainshock [5]. According to the field report made by National Institute for Land and Infrastructure Management (NILIM) and Building Research Institute (BRI) (2016), more than 80% damage ratio of wooden houses had been reported in several 100 meter survey grids in Mashiki [1]. The damage area formed a narrow band between the NO.28 local road and the Akizu river which passes through Downtown Mashiki from east to west [6], as shown in Fig. 1.

Fig. 1. Building damage survey results of the AIJ [7]. The heavy damage percentage of each grid was the ratio of number of heavily damaged buildings in the grid over the number of all the buildings in the grid. Grids filled with green, yellow, orange, red and dark red color represented heavy damage percentage of 0%, 0% - 25%, 25% - 50%, 50% - 75% and more than 75%, respectively. The dotted line is rough outline of heavy building damage area. Big star markers are strong-motion stations in Mashiki Town. The “Site K” which is marked as black dot is a borehole drilling site referenced to Arai (2017) [8].

Similar to the special damage belt in Mashiki after the mainshock of the 2016 Kumamoto earthquake, it also formed a building damage belt in Kobe city after the 1995 Hyogo-ken Nanbu (Kobe) earthquake. Kawase proposed that the region with both high PGA and high PGV corresponds to the special damage belt in Kobe city[9]. Whether the spatial building damage belt at Mashiki also has relationships with the PGA and PGV distribution or not, we need to do father study.

There are two strong motion stations in Mashiki Town. One is the KMMH16, a KiK-net station set by the National Research Institute for Earth Science and Disaster Resilience (NIED), which is located at the north boundary of Downtown Mashiki. Another is set by the Instrumental Intensity Seismometer (IIS) of

Kumamoto Prefecture, we describe this site as KMMP58, which is located on the first floor of the Mashiki Town Hull (a 3 floor RC building) [1]. We obtained the earthquake waves during the mainshock at these two stations. the peak ground velocity (PGV) of EW component of the mainshock observed at KMMP58 was 176 cm/s and PGV observed at KMMH16 was 133 cm/s, the peak ground acceleration (PGA) at KMMP58 was 825 cm/s^2 and PGA observed at KMMH16 was 1160 cm/s^2. As shown in Fig. 1, the distance between KMMH16 and KMMP58 is only about 680m, why the PGA and PGV had so much different in such a small area? We want to know whether the site effects was one reason to explain that.

To understand the site effects of Mashiki, we did the microtremor observation in and around the damage ratio belt at Mashiki after the mainshock (Fig. 2). We analyzed their Microtremor Horizontal-to-Vertical Spectral Ratios (MHVR). Then we transfered the MHVR to the Earthquake Horizontal-to-Vertical Spectral ratio (EHVR) by using the EMR method [2, 10]. Then, we identified the subsurface velocity structure of Mashiki using the diffuse field concept (DFC) and the hybrid heuristic search [3, 10, 11]. Next, we did dynamic seismic response of the identified structures with the linear analysis method (LA) and equivalent linear analysis method (ELA) [12, 13]. Finally, we compared the PGA and PGV distribution maps with the building damage ratio distribution [1, 6, 7].

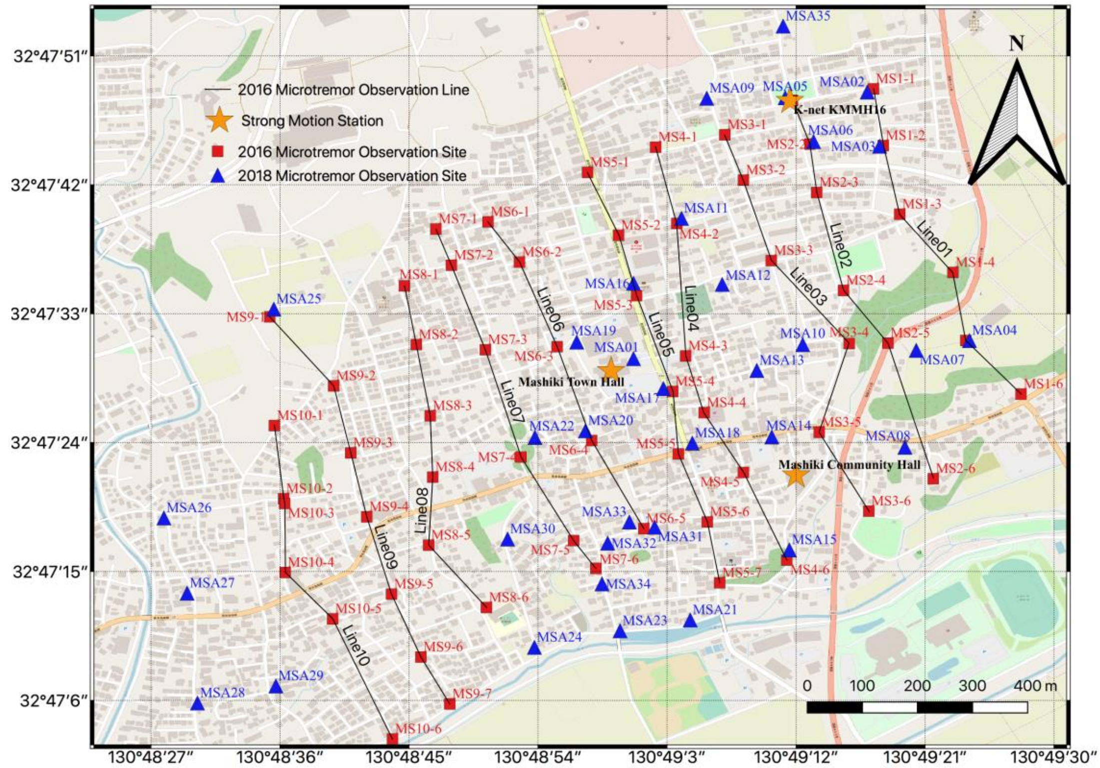

Fig. 2. Microtremor observation sites conducted in 2016 and 2018. Rectangle markers stand for site locations of the 2016 microtremor observation at 61 sites. Triangle markers represent site locations of the 2018 microtremor observation at 35 sites. The big star markers are the locations of three strong-motion stations in this area which were managed by NIED and Kumamoto Prefecture. Solid lines are the ten observation routes during the 2016 microtremor observation.

2. Microtremor Observation

From April 29th to May 1st, 2016, we conducted the first-time microtremor measurement in and around the building dmage area at Downtown Mashiki. During this observation, we used 10 sets of microtremor observation system. We used SMAR-6A3P which is three component accelerometer manufactured by the

Akashi Corporation combined with data logger LS-8800 made by Hakusan Corporation. We obtained 61 microtremor waves in those three days [1], as shown in Fig. 2, the red rectangles represented their locations. For the 2016 microtremor observation sites, we called them as “MS L-X”, “MS” means the observation sites were located at the Downtown Mashiki, “L” means the number of the observation line from 01 to 10, “X” means the observation order along each observation line from north to south.

We can also find the some observation lines were not straight lines in Fig. 2, the reason was we could not reach the preplanned observation sites because of the damaged buildings and retaining walls. Therefore, we conducted the second-time microtremor observation after local citizens moved obstacles. From Jun 3rd to Jun 4th, 2018, we obtained another 35 microtremor waves at Mashiki using the same observation equipment to the first observation, marked as blue triangles in Fig. 2. We called the 2018 microtremor observation sites as “MSAxx”, “MSA” means additional microtremor observation sites at Downtown Mashiki, “xx” was the observation sequence in 2018.

After we got these microtremor waves in Mashiki, we analyzed the MHVR following these steps. First, we divided microtremor waves into 40.96 segments with 50% overlap. Second, we get the Fourier spectrum by the Fast Fourier Transform method (FFT) with Parzen window smoothing of 0.1 Hz width. Third, we discarded the spectrums of noisy sections whose characteristics were much different from the microtremor spectrums of quiet sections. Fouth, we calculated the spectral ratio of the horizontal component with respect to the vertical one, in which we get both the independent ratios of EW/UD and NS/UD and the root mean square (RMS) value of these two ratios by Eq. (1). At last, we calculated the average values of MHVRs as the MHVR of one site. We showed some MHVRs in Fig. 3. We obtained the peak frequencies of MHVRs at most of the observation sites. According to some research results, this peak frequency equals to the predominant frequency of the observation sites [14 – 16]. The peak frequencies are larger in northeast and are lower at the southwest where is near the Akizu River (as shown in Fig. 4).

$$MHVR(RMS) = \sqrt{\frac{[MHVR(EW/UD)]^2 + [MHVR(NS/UD)]^2}{2}} \tag{1}$$

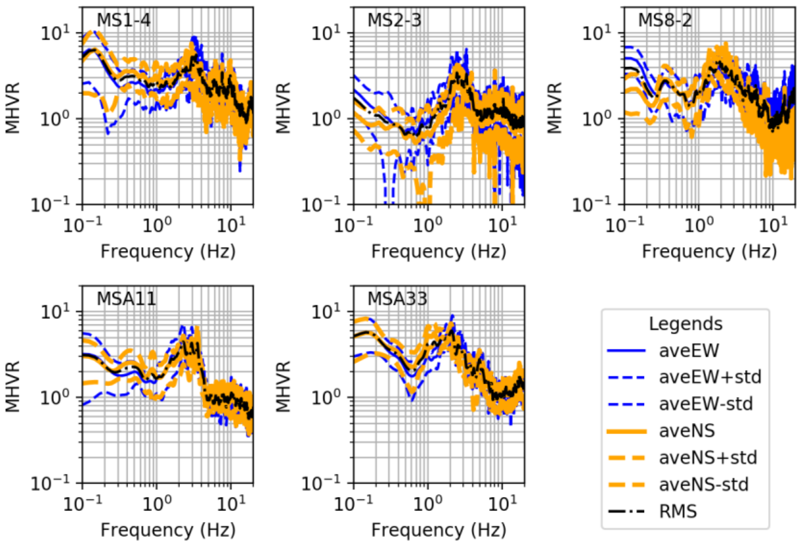

Fig. 3. MHVRs of five microtremor observation sites. Three sites were observed in 2016 and two sites were observed in 2018. The thin solid line in each panel stands for the MHVR of the EW component; the thin dash lines represent the average value plus/minus standard deviation of the EW component. The heavy solid and

heavy dash lines in each panel stand for those of the NS component. The dash-dot lines stand for the root mean square values of the averaged EW and NS components.

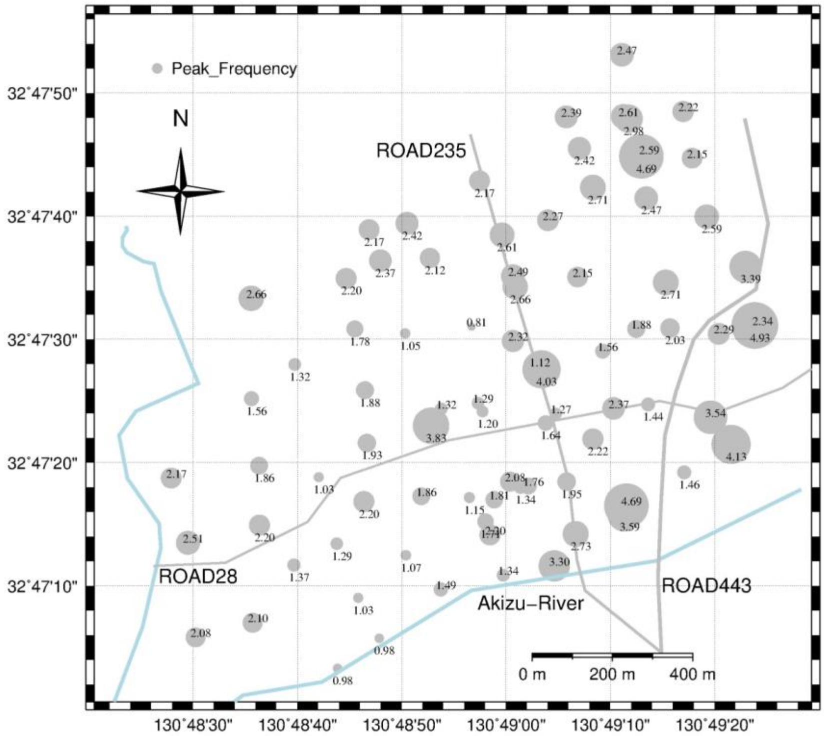

Fig. 4. Predominant frequency distribution map of microtremor observation sites. A larger grey circle means that the predominant frequency of this site is higher.

4. The EMR Method

Kawase et al. (2018a) proposed the EMR method to convert MHVR to EHVR, as the inversion for the EHVR is much more efficient than the MHVR [2, 10]. however, it is easier to obtain MHVR for us because we need to take continuous observation of strong ground motion for a long period to get EHVR. MHVR and EHVR are similar to each other until the fundamental frequency at one site, but they showed difference in the frequency range higher than the peak frequency of MHVR. EMRs are simply the ratios between EHVR and MHVR, using Eq. (2). They divided EMRs into five categories based on the peak frequency of MHVR and EMR is averaged in each category. Those five categories were: 0.2 – 1.0 Hz, 1.0 – 2.0 Hz, 2.0 - 5.0 Hz, 5.0 – 10.0 Hz and 10.0 – 20.0 Hz, as shown in Fig. 5. We can calculate the pseudo-EHVR (pEHVR) using Eq. (3).

$$EMR = \frac{EHVR}{MHVR} \tag{2}$$

$$pEHVR = MHVR \times EMR \tag{3}$$

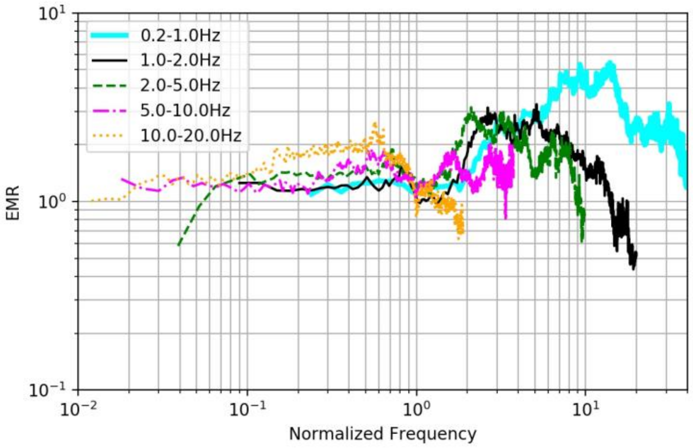

Fig. 5. Five categories of EMRs [2]. The cyan solid line, black thin line, green dashed line, magenta dash-dot line and orange dotted line are the EMR whose peak frequency is located in between 0.2 Hz and 1.0 Hz, 1.0 Hz and 2.0 Hz, 2.0 Hz-5.0 Hz, 5.0 Hz-10.0 Hz and 10.0 Hz-20.0 Hz, respectively.

5. Velocity Structure Inversion

Diffused field concept for earthquakes assuming plane body waves was proposed by Kawase et al. (2011). They derived the theoretical formula for EHVR using Eq. (4). The α_H and β_H are the P- and S-wave velocities of the half-space, respectively. One important notice is that we need to consider the whole velocity structure down to the seismological bedrock in EHVR.

$$\frac{H(0,\omega)}{V(0,\omega)} = \sqrt{\frac{\mathrm{Im}[G^{Earthquake}_{Horizontal}(0,0;\omega)]}{\mathrm{Im}[G^{Earthquake}_{Vertical}(0,0;\omega)]}} = \sqrt{\frac{\alpha_H}{\beta_H}}\frac{|TF_{Horizontal}(0,\omega)|}{|TF_{Vertical}(0,\omega)|} \tag{4}$$

With the theory of EHVR from the DFC for earthquake, Nagashima et al. (2014) proposed a scheme to invert a velocity structure [3]. In this research, we assumed the damping ratio as 1.1% for all the layers and we minimized the misfit between target EHVR and synthetic EHVR by Eq. (5). The HVR_{OBS} means the target EHVR or pEHVR, $EHVR_{SYN}$ means the synthetic EHVR calculated by the DFC for earthquakes. f_{min} and f_{max} mean the minimum and maximum frequency to calculate Eq. (5), in this research f_{min} equals to 0.3 Hz and f_{max} equals to 20 Hz. The increment of frequency is equal in logarithmic scale. For the density of each layer we use Eq. (6). The initial model was shown in Table 1.

$$Misfit = \sum_{f\,\min}^{f\,\max}[\log(EHVR_{OBS}(f)) - \log(EHVR_{SYN}(f))]^2 \tag{5}$$

$$\rho = 1.4 + 0.67 \times \sqrt{\frac{V_S}{1000}} \tag{6}$$

We inverted velocity structures at microtremors observation sites to reproduce their pEHVRs. we did ten trials of EHVR inversion for each site with the different random number seeds. For each inversion, we set the thickness of 1st to 8th layer could be changed in a searching range and kept the Vs and Vp the same as the initial model. Thus, we identified the velocity structures for the following nine cases.

1) The searching range of thickness for the 1st – 8th layer as 100%. Keep their Vs, Vp the same as the initial model.

2) The searching range of thickness for the 1st – 8th layer as 200%. Keep their Vs, Vp the same as the initial model.

3) The searching range of thickness for the 1st – 8th layer as 300%. Keep their Vs, Vp the same as the initial model.

4) The searching range of thickness for the 1st – 8th layer as 400%. Keep their Vs, Vp the same as the initial model.

5) The searching range of thickness for the 1st – 4th layer as 200% and the searching range of thickness for the 5th – 8th layer as 100%. Keep their Vs, Vp the same as the initial model.

6) The searching range of thickness for the 1st – 4th layer as 300% and the searching range of thickness for the 5th – 8th layer as 100%. Keep their Vs, Vp the same as the initial model.

7) The searching range of thickness for the 1st – 4th layer as 400% and the searching range of thickness for the 5th – 8th layer as 100%. Keep their Vs, Vp the same as the initial model.

8) The searching range of thickness for the 1st – 4th layer as 300% and the searching range of thickness for the 5th – 8th layer as 200%. Keep their Vs, Vp the same as the initial model.

9) The searching range of thickness for the 1st – 4th layer as 400% and the searching range of thickness for the 5th – 8th layer as 200%. Keep the Vs, Vp as the initial model of each layer.

Table1.

The reference model of pEHVR inversion at Mashiki Town. This model is also the best-fit model of EHVR inversion at KMMH16 [17].

Layer Number	Thickness (m)	Depth (m)	Vp (m/s)	Vs (m/s)	Density (g/cm3)
1	3.00	3.00	296.56	154.87	1.66
2	12.00	15.00	760.00	249.36	1.73
3	5.29	20.29	1841.61	337.07	1.79
4	2.10	22.39	1918.07	483.09	1.87
5	15.80	38.19	1995.00	598.03	1.92
6	12.50	50.69	1995.09	733.19	1.97
7	25.30	75.99	2529.23	790.10	2.00
8	16.13	92.12	2558.47	827.70	2.01
9	44.92	137.04	2768.98	990.51	2.07
10	29.23	166.27	4078.39	1172.19	2.13
11	64.60	230.87	4796.23	1468.35	2.21
12	15.52	246.39	4813.21	1790.20	2.30
13	905.78	1152.17	5776.98	1871.20	2.32
14	3100.31	4252.48	5786.36	3264.74	2.61
15	0.00	4252.48	6000.00	3400.00	2.64

Among these nine cases, the smaller searching range of thickness will lead to the smaller inclinations of subsurface layers between two microtremor observation sites. But the misfit between target EHVR and synthetic EHVR will also be larger at the same time. Considering above viewpoints, we choose the identification results of case 5 as the best for this research. Fig. 6 shows identification results of three sites in case 5. At these sites the inversion results among ten trials converged to the same velocity structures.

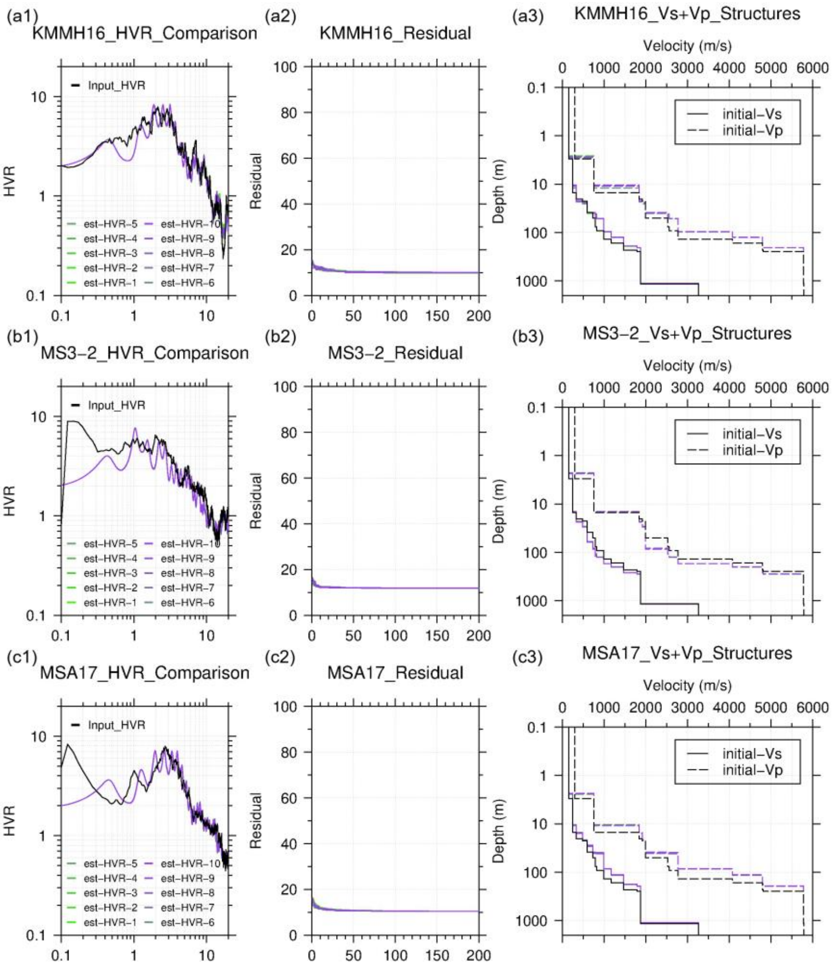

Fig. 6. Velocity structure identification results of three sites. (a1) is the comparison of synthetic HVR and target EHVR of KMMH16, the black line represents the target EHVR-KMMH16; (a2) is residual convergence between the synthetic HVR and the target EHVR of KMMH16 from 0.3Hz to 20Hz for ten trials; (a3) is comparison of initial Vs and Vp velocity models with ten identified Vs and Vp velocity structures of KMMH16, the black solid line represents the initial Vs model and the black dash line represents the initial Vp model. Similarly, (b1), (b2) and (b3) are those of the MS3-2 site. (c1), (c2) and (c3) are those of the MSA17 site.

6. Dynamic Response Analysis in Mashiki

After we got the subsurface structure, we analyzed the dynamic response of every microtremor observation site and every strong-motion station. We tried to use both the Linear Analysis (LA) method and the Equivalent Linear Analysis (ELA) method [12, 13].

In the ELA method, nonlinear soil properties of subsurface layers are important. According to the experimental results of borehole drilling at Mashiki [8], we obtained the relationship between shear strain (γ) and shear modulus ratio (G/G_{max}) and the relationship between γ and damping ratio (h) for three kinds of soils (Clay1, Sand1 and Sand2) at site K. For the nonlinear parameters of gravel layer, we cited Imazu and Fukutake (1986) [18]. We showed the nonlinear soil parameters in Fig. 7.

When we did the dynamic response of subsurface layers, we need the input wave to seismological bedrock during the mainshock of Kumamoto Earthquake. Nagashima et al. (2017) attempted to estimate the horizontal seismic bedrock motions from the observed vertical strong ground motions based on the DFC for earthquakes [19]. In the actual calculation of the bedrock motions at KMMH16 in Nagashima et al. (2018), they applied Eq. (6) to the early coda immediately after the main part of S-wave to calculate nonlinear horizontal transfer function [17].

$$TF_{horizontal}^{Nonlinear} = Spectra_{horizontal} \times \left(\sqrt{\frac{\alpha}{\beta}} \times \frac{Spectra_{vertical}}{TF_{vertical}}\right)^{-1} \tag{6}$$

By assuming that this nonlinear transfer function of the early coda would keep the same shape during the strong shaking and deconvolving the whole wave of P-wave, S-wave and coda by the estimated transfer function, the seismological bedrock wave can be obtained. We used the estimated seismic waves at seismological bedrock of KMMH16 reference to Nagashima et al. (2018). Combining with the research results of Arai (2017) and the borehole logging data of KMMH16, we decided the nonlinear soil property based on Vs and Vp.

After obtaining soil properties, seismic bedrock motions, and soil material characteristics mentioned above, we firstly performed the linear and equivalent linear analyses at KMMH16 by the "DYNEQ" software [12, 13]. We showed the dynamic response results of EW component in Fig. 8. Also, the maximum shear strain of the ELA analysis result was less than 1%. Thus, we think the ELA was applicable to KMMH16the dataset in this research. Then we carried out ELA at the microtremor observation sites and obtained the estimated PGA and PGV of every site. In Fig. 9, the PGV distribution showed close correlation to the building damage belt in Mashiki, while the PGA distribution did not show close correlation with the building damage belt.

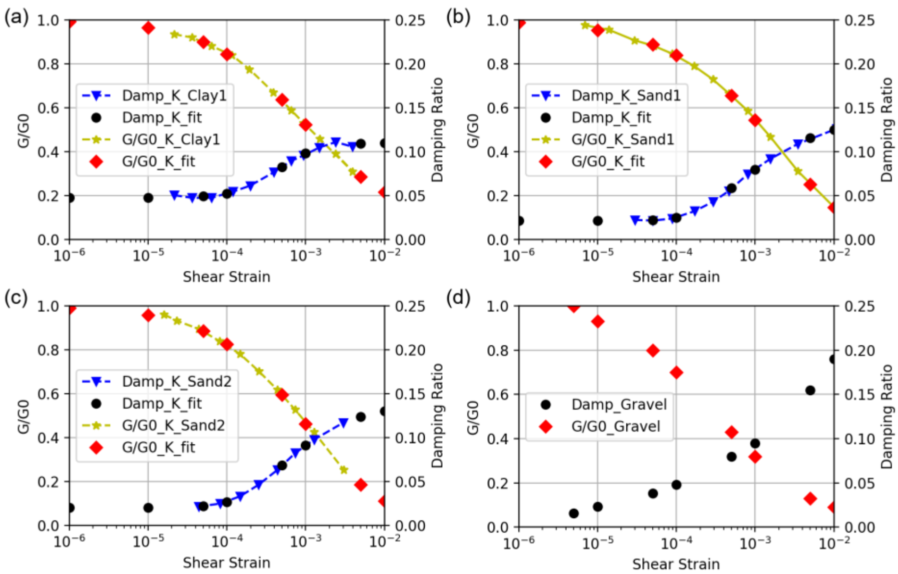

Fig. 7. Four kinds of nonlinear soil properties. The (a), (b), (c) figures are interpolated soil nonlinear properties at 'site K' reference to the experimental data of Arai (2017). (a) is the soil property of 'Clay 1', (b) is the soil property of 'Sand 1', (c) is the soil property of 'Sand 2' and (d) shows soil property of gravel which was referred to Imazu and Fukutake (1986). In (a), (b) and (c), the dash lines with star markers are

experimental data of "G/G_{max} - Shear Strain", the dash lines with inverted triangles are experimental data of "Damping Ratio - Shear Strain", the diamond markers are interpolated results of "G/G_{max} - Shear Strain" and the circle markers are interpolated results of "Damping Ratio - Shear Strain" that we used in ELA. In (d), the diamond markers are interpolated results of "G/G_{max} - Shear Strain" and the circle markers are interpolated results of "Damping Ratio - Shear Strain" that we used in ELA for gravel material.

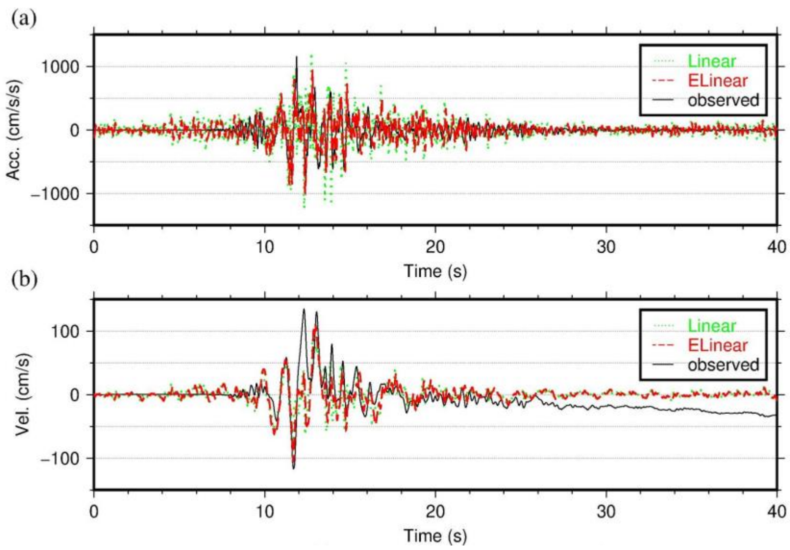

Fig. 8. The estimated ground surface acceleration and velocity of EW component at KMMH16 during the mainshock using LA and ELA. (a) is the estimated ground acceleration of LA (dotted green line) and ELA (dash red line), comparing with the observed strong ground motion (solid black line), the unit is "cm/s^2". (b) is the estimated ground velocity of LA (dotted green line) and ELA (dash red line), comparing with the ground velocity integrated from the observed acceleration (solid black line), the unit is "cm/s".

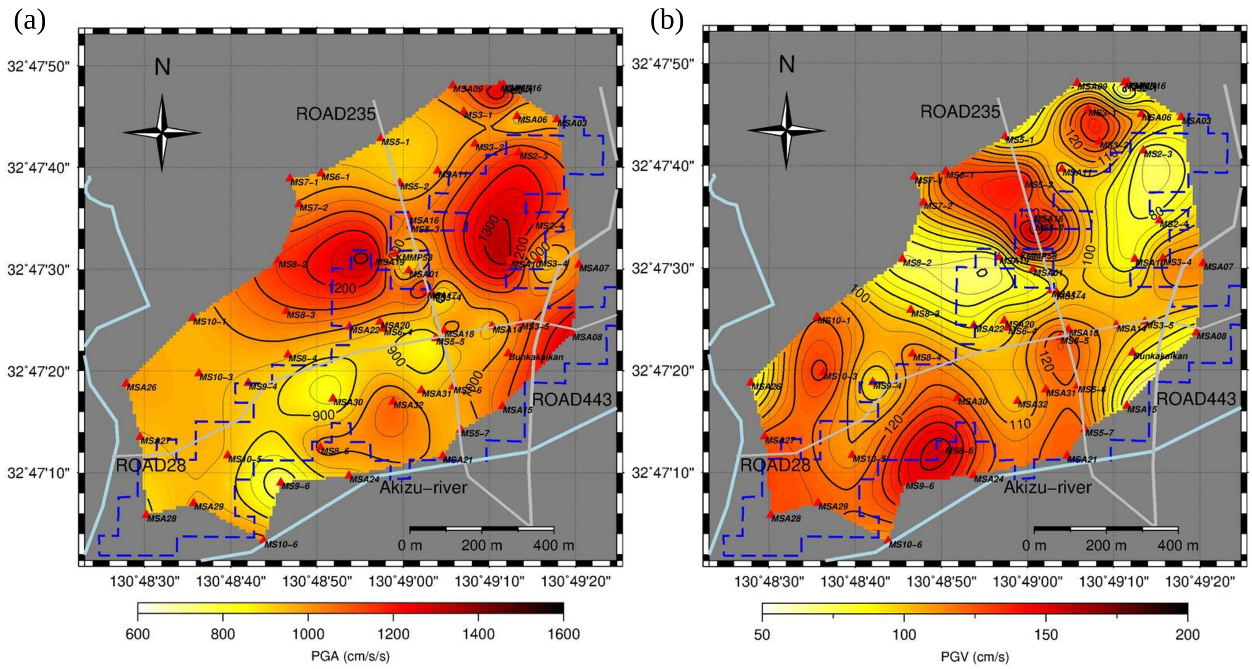

Fig. 9. PGA (a) and PGV (b) distribution map of ELA for the EW component. The blue dash line is outline of the building damage belt area in Mashiki. The unit of PGA is "cm/s^2", the unit of PGV is "cm/s".

7. Conclusion

Based on the peak frequency of MHVR, we found that the peak frequency of MHVR at the area near the Akizu River (southwestern part of Mashiki) is smaller than 1.0 Hz. The peak frequency of northeastern part was higher than the southwestern part.
The EMR method could be used in Mashiki area. The pEHVR is good enouth to identify the velocity structures based on the DFC for earthquakes at Mashiki.
According to the linear analysis results and the equivalent linear analysis results at KMMH16 in both the EW and NS components, the linear results showed that the acceleration was overestimated while the equivalent linear results showed that both the estimated acceleration and velocity waveforms were reproduced the observed waves quite well at KMMH16.
According to the distribution map of estimated PGV and PGA, we consider the PGV distribution map of the ELA case corresponds to the building damage belt distribution at Mashiki.

8 Acknowledgements

We want to say thank you to all the team members of Kawase and Matsushima laboratory who helped microtremor observation in 2016. We also want to express our gratitude for the help of the Kumamoto Prefecture, JMA, and NIED who shared with us the important observed strong ground motions at Mashiki Town Hall, Bunkakaikan, and KMMH16. We also appreciate the help of the AIJ research teams and the BRI survey team, who shared with us the survey data of the building damages as well as the soil properties at Mashiki.

References

[1] H. Kawase, S. Matsushima, F. Nagashima, Baoyintu, and K. Nakano, “The cause of heavy damage concentration in downtown Mashiki inferred from observed data and field survey of the 2016 Kumamoto earthquake,” *Earth Planets Space*, vol. 69, no. 1, p. 3, Dec. 2017.

[2] H. Kawase, Y. Mori, and F. Nagashima, “Difference of horizontal-to-vertical spectral ratios of observed earthquakes and microtremors and its application to S-wave velocity inversion based on the diffuse field concept,” *Earth, Planets and Space*, vol. 70, no. 1, p. 1, Jan. 2018.

[3] F. Nagashima *et al.*, “Application of Horizontal-to-Vertical Spectral Ratios of Earthquake Ground Motions to Identify Subsurface Structures at and around the K-NET Site in Tohoku, Japan,” *Bulletin of the Seismological Society of America*, vol. 104, no. 5, pp. 2288–2302, Oct. 2014.

[4] A. Kato, J. Fukuda, S. Nakagawa, and K. Obara, “Foreshock migration preceding the 2016 M_w 7.0 Kumamoto earthquake, Japan: FORESHOCK MIGRATION,” *Geophysical Research Letters*, vol. 43, no. 17, pp. 8945–8953, Sep. 2016.

[5] K. Goda *et al.*, “The 2016 Kumamoto Earthquakes: Cascading Geological Hazards and Compounding Risks,” *Frontiers in Built Environment*, vol. 2, no. 19, Aug. 2016.

[6] M. Yamada, J. Ohmura, and H. Goto, “Wooden Building Damage Analysis in Mashiki Town for the 2016 Kumamoto Earthquakes on April 14 and 16,” *Earthquake Spectra*, vol. 33, no. 4, pp. 1555–1572, Nov. 2017.

[7] NILIM and BRI, “Quick Report of the Field Survey and the Building Damage by the 2016 Kumamoto Earthquake,”, https://www.kenken.go.jp/japanese/contents/publications/data/173/index.html, last accessed Jan. 2020 [Japanese].

[8] H. Arai, “Influence of ground characteristics in the center of Mashiki-cho on strong ground motion in the 2016 Kumamoto earthquake.” *BRI-H29 lecture*, 2017.

[9] H. Kawase, “The Cause of the Damage Belt in Kobe: ‘The Basin-Edge Effect,’ Constructive Interference of the Direct S-Wave with the Basin-Induced Diffracted/Rayleigh Waves,” *Seismological Research Letters*, vol. 67, no. 5, pp. 25–34, Sep. 1996.

[10] H. Kawase, F. J. Sanchez-Sesma, and S. Matsushima, “The Optimal Use of Horizontal-to-Vertical Spectral Ratios of Earthquake Motions for Velocity Inversions Based on Diffuse-Field Theory for Plane Waves,” *Bulletin of the Seismological Society of America*, vol. 101, no. 5, pp. 2001–2014, Oct. 2011.

[11] H. Yamanaka, “Inversion of surface-wave phase velocity using hybrid heuristic search method,” *BUTSURI-TANSA*, vol. 60, no. 3, pp. 265–275, 2007.

[12] N. Yoshida, "DYNEQ - A computer program for Dynamic response analysis of level ground by Equivalent Linear Method." , https://www.kiso.co.jp/yoshida/English_02.html , last accessed Jan. 2020.
[13] N. Yoshida and S. Iai, Nonlinear site response and its evaluation and prediction, *Proc. 2nd International Symposium on the Effect of Surface Geology on Seismic Motion,* Yokosuka, Japan, Vol. 1, pp. 71-90, 1998.
[14] K. Konno and T. Ohmachi, "Ground-Motion Characteristics Estimated from Spectral Ratio between Horizontal and Vertical Components of Microtremor," *Bulletin of the Seismological Society of America*, vol. 88, no. 1, pp. 228–241, Feb. 1998.
[15] P.-Y. Bard, *Microtremor measurements: A tool for site effect estimation?*, vol. 3. 1999.
[16] T. Satoh *et al.*, "S-Wave Velocity Structure of the Taichung Basin, Taiwan, Estimated from Array and Single-Station Records of Microtremors," *Bulletin of the Seismological Society of America*, vol. 91, no. 5, pp. 1267–1282, Oct. 2001.
[17] F. Nagashima and H. Kawase, "Estimation of the incident spectrum at the seismic bedrock by using the observed vertical motion at the ground surface based on diffuse field theory," presented at *the Proceedings of the 15th Japan Earthquake Engineering Symposium*, 2018.
[18] M. Imazu and K. Fukutake, "A Study on Data Processing of Dynamic Deformation Properties," *The 21st Geotechnical Engineering Conference of Japan*, pp. 603–604, 1986.
[19] F. Nagashima, H. Kawase, and S. Matsushima, "ESTIMATION OF HORIZONTAL SEISMIC BEDROCK MOTION FROM VERTICAL SURFACE MOTION BASED ON HORIZONTAL-TO-VERTICAL SPECTRAL RATIOS OF EARTHQUAKE MOTIONS," in *16th World Conference on Earthquake*, 2017, p. 10.

